*Journal of Hydraulic Research* Vol. 44, No. 6 (2006), pp. 841–856


# Prediction of contaminant plumes (shapes, spatial moments and macrodispersion) in aquifers with insufficient geological information

# Prévision des panaches de contaminant (formes, moments spatiaux et macrodispersion) dans les couches aquifères manquant d'information géologique

AMRO M.M. ELFEKI*, *Water Resources Section, Department of Water Management, TU Delft, PO Box 5048, 2600 GA Delft, The Netherlands. E-mail: amro_elfeki@yahoo.com (Present address: Water Resources Department Faculty of Meteorology, Environment and Arid Land Agriculture, King Abdulaziz University, Jeddah, Saudi Arabia)*

**ABSTRACT**
The first Macrodispersion Experiment (MADE1) at Columbus Air Force Base in northern Mississippi is utilized to perform numerical simulations of solute transport in an aquifer. The purpose is to illustrate the capability of the coupled Markov chain (CMC) model in delineating the complex geometrical configuration at the site for solute transport simulations under the lack of geological information. The CMC model is also used to study the effect of reducing geological information on the transport predictions in terms of plume configuration, first and second spatial moments and macrodispersion. The results show the power of the coupled Markov chain methodology in delineating aquifer heterogeneity at the site. Conditional simulations on 16, 9 and 6 boreholes show reasonably the same plume behavior in terms of average longitudinal and vertical extensions, especially in the far-field; 9 boreholes seem to provide practically acceptable results in terms of the global plume shape. This indicates more reliability on the use of the CMC model for subsurface characterization. Comparison of CMC model results, in terms of aquifer characterization, with the model used by Eggleston and Rojstaczer [Water Resour. Res. 34 (1998) 2155] (polynomial regression trend, Kalman filter trend, hydrofacies trend and Kriging) shows that the CMC model behaves better. The CMC model conditioned on 9 and 16 boreholes with mid-range conductivities for each lithology captures both the plume shape and the observed plume spatial moments at the MADE site.

**RÉSUMÉ**
Le premier site expérimental de macrodispersion (MADE1) à la base aérienne de Columbus au nord du Mississippi est utilisé pour effectuer des simulations numériques de transport de corps dissous dans une couche aquifère. Le but est d'illustrer la capacité du modèle de chaîne de Markov couplée (CMC) à traçer la configuration géométrique complexe sur le site des simulations de transport de corps dissous malgré un manque d'information géologique. Le modèle CMC est également utilisé pour étudier l'effet d'une réduction de l'information géologique sur les prévisions de transport en termes de configuration de panache, de premier et second moments spatiaux et de macrodispersion. Les résultats montrent la puissance de la méthodologie de la chaîne de Markov couplée dans la détermination de l'hétérogénéité de la couche aquifère sur le site. Des simulations conditionnelles effectuées sur 16, 9 et 6 forages montrent raisonnablement le même comportement de panache en termes d'extensions longitudinales et verticales moyennes, particulièrement dans le champ éloigné ; 9 forages semblent fournir des résultats pratiquement acceptables en termes de forme globale de panache. Ceci indique plus de fiabilité sur l'utilisation du modèle CMC pour la caractérisation du sous-sol. La comparaison des résultats du modèle CMC, en termes de caractérisation de la couche aquifère, montre que le modèle CMC se comporte mieux, d'après Eggleston et Rojstaczer [Water Resour. Res. 34 (1998) 2155] en utilisant différents modèles (polynôme de régression, filtre de Kalman, hydrofaciès et Kriging). Le modèle CMC conditionné sur 9 et 16 forages, avec des conductivités médianes pour chaque lithologie, capture à la fois la forme et les moments spatiaux du panache observé sur le site MADE.

*Keywords*: Heterogeneity, conditioning, flow, transport, field data, Markov chains.

## 1 Introduction

A large-scale natural-gradient macrodispersion test (Boggs *et al.*, 1990, 1992) was conducted at the Columbus Air Force Base in Mississippi. The primary objectives of the experiment include: (1) providing estimates of macrodispersivities (for the advection–dispersion model) for the comparison with those estimated from spatial moments analysis and stochastic theories; (2) developing a field-scale benchmark problem for testing numerical codes and alternative transport theories; (3) understanding the role of aquifer heterogeneity in controlling contaminant fate and transport; and (4) evaluating the effectiveness of

*On leave from Civil Engineering Dept., Faculty of Engineering, Mansoura University, Mansoura, Egypt.
Revision received October 4, 2005/Open for discussion until June 30, 2007.

various geostatistical approaches for constructing the hydraulic conductivity distribution from field data.

Eggleston and Rojstaczer (1998) have applied various deterministic and geostatistical methods (e.g. polynomial regression, Kalman filtering, sedimentation zone and Kriging) to identify trends in the hydraulic conductivity fields at the macrodispersion experiment (MADE) site. The methods show significant differences in both modeling the spatial variability and the effect on transport. They conclude that even with nearly 2500 hydraulic conductivity measurements, it is not possible to unambiguously identify large-scale variability controlling advective transport at the MADE site. Zheng and Jiao (1998) pointed out the need for new innovative techniques (e.g. advanced seismic methods) that can be applied to characterize the spatial and temporal variabilities in aquifer parameters.

Elfeki and Rajabiani (2002) have applied the coupled Markov chain (CMC) methodology developed by Elfeki and Dekking (2001) at the MADE site. The objective was to investigate how the CMC model is capable of characterizing heterogeneity at this site. The results are promising. The method is capable of capturing the dominant heterogeneities in the site when conditioned on the given data (16 boreholes).

The objective of this paper is to elaborate the work by Elfeki and Rajabiani (2002), where they only considered plume shapes. This paper investigates how lack of geological information influence transport predictions in terms not only of plume shapes but also of plume spatial moments, evolution of macrodispersion, macrodispersivity, and breakthrough curves at the MADE site. Comparison between results in this study and results of research work reported in the literature are also presented.

## 2 Description of the MADE1 experiment

A field tracer experiment, called the MADE1 (first Macrodispersion Experiment), was performed at Columbus Air Force Base in northeastern Mississippi (Rehfeldt *et al.*, 1992). The shallow unconfined aquifer that immediately underlines the site consists of an alluvial terrace deposit averaging approximately 11 m in thickness. The aquifer is composed of poorly sorted to well-sorted sandy gravel and gravelly sand with minor amounts of silt and clay. Soil mapping investigations adjacent to the site indicated that soil facies occur as irregular lenses and layers having horizontal dimensions ranging up to 8 m and vertical dimensions of less than 1 m. The spatial distribution of the hydraulic conductivity at the site was determined from 2187 measurements in 16 fully penetrating wells. For a full description of the site, reference is made to Rehfeldt *et al.* (1992) and Boggs *et al.* (1990, 1992). It is concluded from the site investigation that the Columbus site is distinct from previous natural gradient experiments in the literature because of the extreme heterogeneity of the aquifer. Its heterogeneity (in terms of the variance of the logarithm of hydraulic conductivity) is at least an order of magnitude larger than aquifers at other sites such as Borden, Ontario, Canada (Sudicky, 1986) and Cape Cod, Massachusetts, USA (Hess *et al.*, 1992). It also has large-scale spatial variations in groundwater velocity for the aquifer.

The hydraulic head field at the site exhibits complex temporal and spatial variability that is accounted for by the heterogeneity of the aquifer and large seasonal fluctuations of the water table. The flow field showed a converging groundwater flow toward a narrow zone of relatively high mean conductivity and an increasing groundwater velocity in the zone of convergence as shown in Adams and Gelhar (1992). The converging groundwater flow field in the vicinity of the test site played an important role in the evolution of the tracer plume. General trends have been observed from the water table maps at the site. In the far-field region of the test site there is relatively high mean conductivity (i.e., of the order of $10^{-2}$–$10^{-1}$ cm/s) corresponding to widely spaced hydraulic head contours, whereas the closely spaced contours in the near-field indicate relatively low mean conductivity (i.e., of the order of $10^{-3}$ cm/s). These trends are consistent with the borehole flowmeter measurements of hydraulic conductivity (Boggs *et al.*, 1990, 1992). The specific yield estimates for the tests indicate that the aquifer is unconfined to semi-confined.

A conservative bromide tracer in the form of $CaBr_2$ was utilized as the primary tracer. The tracer was injected as a uniform pulse released into approximately the middle of the saturated zone with a minimal amount of disturbance to the natural flow field (Boggs *et al.*, 1990, 1992). Over a period of 48.5 h, 10.07 $m^3$ of groundwater containing 2500 mg/L of bromide was injected at a uniform rate. The monitoring method used at the site is multilevel samplers to provide water samples from discrete zones in the aquifer. Concentration maps of vertically averaged bromide plumes and vertical cross-sections are presented in Adams and Gelhar (1992).

In the current study, the focus is on plume presentation in vertical cross-sections. Snapshots of Bromide plumes at 49, 279 and 594 days since release are shown in Fig. 1. The salient features of the bromide plumes can be summarized as: (1) Skewness of the concentration distribution in the longitudinal direction where the peak concentration is located near the injection zone. This is due to the relatively low mean conductivity (i.e., approximately $10^{-3}$ cm/s) at the near-field where the main body of the plume is moving with relatively slow velocity (5–10 m/year). (2) Most of the tracer stays close to the injection well. (3) Unexpectedly large vertical spreading of the plume. This can be attributed to three causes. Firstly, the artificial vertical gradient created by tracer injection. Secondly, the natural upward vertical gradients present in the vicinity of the injection site. Thirdly, the density difference, since the tracer solution is approximately 0.4% denser than ambient groundwater it may contribute to the downward spreading of the plume. (4) Maximum bromide concentrations of the bromide profile at 594 days were located in the upper part of the plume near the water table. (5) Reduction of the plume thickness that occurred between approximately 20 and 40 m down gradient from the injection point. This is due to natural channeling (preferential flow) through a relatively permeable zone in this region. (6) Vertical extension of the plume down gradient after the observed convergence due to the channeling described in point (5). This is consistent with the downward gradient in the far-field region.

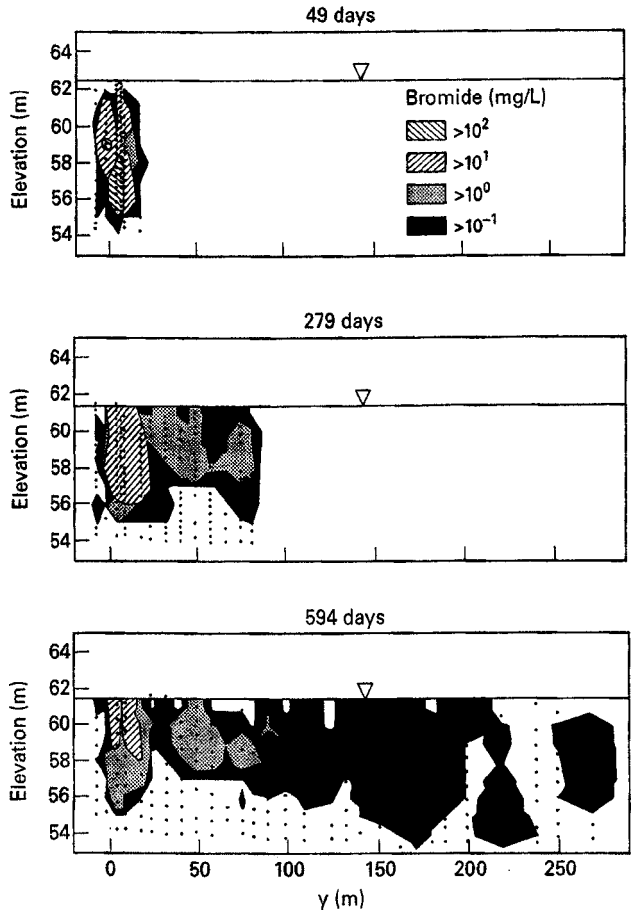


Figure 1 Three snapshots of the bromide plume at 49, 279 and 594 days (Boggs *et al.*, 1990, 1992).

## 3 Application of the 2D-coupled Markov chain model to the MADE site

The CMC model, developed by Elfeki (1996) and extended by Elfeki and Dekking (2001) to conditioning on multiple boreholes, is applied at the MADE site. A brief description of the CMC model is given below. The model is stochastic in nature, and couples two Markov chains. The first one is used to describe the sequence of lithologies in the vertical direction, and the second describes the sequence in the lithological structure in the horizontal direction. The two chains are coupled in the sense that a state of a cell $(i, j)$ in the domain depends on the state of two cells, the one on top $(i, j-1)$ and the other on the left $(i-1, j)$ of the current cell (Fig. 2, top). The model is very general, it can handle any three cells from various directions. We can even have four possibilities namely top and left (as in this case), bottom and left, right and bottom, and right and top. This type of modeling approach is called unilateral Markov random fields (see e.g. Galbraith and Walley, 1976). The reason behind this choice is twofold: first is to develop an efficient generation algorithm of Markovian fields. Traditional Markov random fields (Cross and Jain, 1983) use dependence of four neighboring cells that leads to implicit formulation of the generation algorithm. This procedure becomes inefficient in terms of computer time and does not produce satisfactory results from the geological point of view (see Cross and Jain, 1983). Second is data steering, in field situations data are

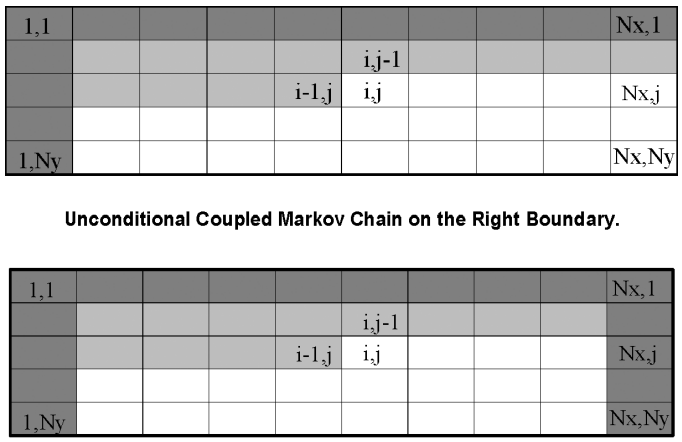


Figure 2 Numbering system in two-dimensional domain for the coupled Markov chain. Unconditional Markov chain (top), and Markov chain conditioned on future states (bottom). Dark grey cells are known boundary cells, light grey cells are known cells inside the domain (previously generated, the past), white cells are unknown cells. The future state used to determine the state of cell $(i, j)$ is the state of cell $(N_x, j)$ (Elfeki and Dekking, 2001).

usually in the form of boreholes (vertical variability) and surface knowledge (horizontal variability) is gained from the geological survey. The technique tries to propagate the knowledge available on the left vertical and top horizontal boundaries through the horizontal and vertical chains, respectively, into the cells inside the domain. Therefore, according to this dependence the transition probabilities from the two chains are coupled to give,

$$p_{lm,kk} := \Pr(Z_{i,j} = S_k | Z_{i-1,j} = S_l, Z_{i,j-1} = S_m) = \frac{p^h_{lk} \cdot p^v_{mk}}{\sum_f p^h_{if} \cdot p^v_{mf}}, \quad k = 1, \ldots, n, \tag{1}$$

where $p_{lm,k}$ is the probability of cell $(i, j)$ is in state $S_k$ given that cell $(i-1, j)$ is in state $S_l$ and cell $(i, j-1)$ is in state $S_m$, $Z_{i,j}$ is the state of cell $(i, j)$, $Z_{i-1,j}$ is the state of cell $(i-1, j)$, $Z_{i,j-1}$ is the state of cell $(i-1, j)$ and $p^h_{lk}$ and $p^v_{mk}$ are the corresponding elements of the horizontal and vertical transition probability matrices.

An extension of the CMC model to enable conditioning on any number of boreholes is achieved in Elfeki and Dekking (2001). The methodology is based on the concept of conditioning a Markov chain on future states (Fig. 2, bottom). The conditioning is performed in an explicit way [i.e. no need for iterative procedure until you reach convergence around the conditioning data point like the method of Markov random field with Metropolis algorithm (Cross and Jain, 1983)]. This makes the methodology efficient in terms of computer time and storage in comparison with other techniques available in the literature. The conditioning formula is given by,

$$p_{lm,k|q} := \Pr(Z_{i,j} = S_k | Z_{i-1,j} = S_l, Z_{i,j-1} = S_m, Z_{N_x,j} = S_q) = \frac{p^h_{lk} \cdot p^{h(N_x-i)}_{kq} \cdot p^v_{mk}}{\sum_f p^h_{lf} \cdot p^{h(N_x-i)}_{fq} \cdot p^v_{mf}}, \quad k = 1, \ldots, n, \tag{2}$$

where $p_{lm,k|q}$ is the probability that cell $(i, j)$ is in state $S_k$ given that cell $(i-1, j)$ is in state $S_l$ and cell $(i, j-1)$ is in state $S_m$ and cell $(N_x, j)$ is in state $S_q$, and $p_{kq}^{h(N_x-i)}$ is the $(N_x - i)$-step horizontal transition probability matrix which is computed by multiplying the one step horizontal transition probability matrix by itself $(N_x - i)$ times.

In the paper, an engineering approach has been utilized to extract a final image from a collection of realizations generated by a Monte Carlo method. The approach is based on generating $M$ realizations of the geological structure given the transition probabilities and the sampling intervals. Combining these realizations, it is possible to construct the areal probability of presence of each lithology (Elfeki and Dekking, 2001). These probability maps show where each lithology is most likely to be present at a certain location. The probability maps are calculated at each cell by counting the number of times one finds a specific lithology at this cell in the $M$ realizations. For example, if cell number (1,1) has clay in 10 out of $M = 30$ realizations, the probability of clay in this cell is 33.33% and so on. From these probabilities a final image of the geological structure is constructed based on the highest probability at a specific cell. A detailed description of the methodology and its applications are given in Elfeki and Dekking (2005). This approach has also been used by Li *et al.* (2004).

The background that motivated this approach is twofold (Elfeki and Dekking, 2005). First is that subsurface structure is a single realization, therefore we tried to extract the most probable image of the subsurface from a collection of realizations. The second is that engineers prefer cost-effective techniques, So, instead of generating many realizations of subsurface structures and perform flow and transport simulations in each realization (the so-called Monte Carlo method), we propose an alternative approach: one summarizes all the generated realizations, and obtains a single most probable image that can be used later as a deterministic image for flow and transport predictions saving a lot of computational costs.

The two-dimensional CMC has not only been applied at the MADE site but at various sites as well, e.g. at an outcrop at Loranca basin, and at Tortola fluvial system in Spain by Elfeki and Dekking (2001), some dykes (Afsluitdijk-Lemmer and Afsluitdijk-Caspar de Roblesdijk part of Waddenzeedijken) in the Netherlands using cone penetration test (CPT) data by Rajabiani (2001), the underlying aquifer system of the Delaware river by Elfeki and Dekking (2005), an unconsolidated aquifer in the Rhine-Meuse delta, the Netherlands by Keshta *et al.* (2004) and El-Arish-Rafaa coastal area, Egypt by Keshta (2003). The CMC model has also been extended just recently to three dimensions by Park *et al.* (2003) and the author foresee further applications.

## 4 Estimation of the coupled Markov chain model parameters

In the MADE site, there are five different types of facies. The facies are described as open work gravel, fine gravel, sand, sandy gravel and sandy clayey gravel that are coded as 1, 2, 3, 4 and 5, respectively (see Fig. 3). It is assumed that the white space above the geological cross-section of Fig. 3a(a) is a hypothetical lithology coded with state number 6 and the space below the section is coded with state number 7. So, in total we deal with seven states, of which two are hypothetical ones. This is necessary to simulate the top and bottom boundaries of the geological section. The domain dimensions are $276 \times 14.2$ m. The vertical transition probability is calculated using a program called WELLLOG, which has been developed by Elfeki and Rajabiani (2002). Table 1 shows $7 \times 7 = 49$ entries of the vertical direction transition probability matrix calculated from 16 boreholes (shown in Fig. 4). These transitions are calculated in the vertical direction from top to bottom over a sampling interval of 0.1 m. This sampling interval is chosen based on the smallest lithological thickness observed in the boreholes to be reproduced in the simulations with minimum computational effort (Elfeki *et al.*, 1997, p. 76). The procedure is as follows. The tally matrix of vertical transitions is obtained by superimposing a vertical line with equidistant points along the borehole with a chosen sampling interval (0.1 m). The transition frequencies between the states are calculated by counting how many times a given state, say $S_l$, is followed by itself or one of the other states, say $S_k$, in the system and then divided by the total number of transitions,

$$p_{lk}^{v} = \frac{T_{lk}^{v}}{\sum_{q=1}^{n} T_{lq}^{v}} \tag{3}$$

where $T_{lk}^{v}$ is the number of observed transitions from $S_l$ to $S_k$ in the vertical direction.

Boreholes usually are insufficient to quantify spatial variability in the lateral directions, not only because of typically sparse lateral spacing, but also because of unknown variations in the depositional lateral directions. A sensitivity analysis is performed to find out the best estimate of the horizontal transition probability matrix. Three horizontal transition probability matrices are assumed to get the best delineation of the aquifer heterogeneity. Tables 2–4 show three different horizontal transition probability matrices. The three matrices are diagonally dominant (i.e. the diagonal elements are greater than the sum of the off-diagonal elements). The degree of diagonal dominancy increases from Table 2 (low-diagonal dominancy) to Table 4 (high-diagonal dominancy). These transitions are applied over a horizontal sampling interval of 3 m. For the choice of the sampling intervals a reference is made to Elfeki *et al.* (1997, p. 76). It is also important to note that Table 3 is identical to the vertical transition probability matrix. This was done on purpose to see whether the vertical transition matrix could be used as an estimate for the horizontal one, utilizing Walther's law in geology (Middleton, 1973 referenced by Parks *et al.*, 2000). Walther's law states that lithologies that are observed in the vertical depositional sequences must also be deposited in adjacent transects at another scale. This law can be interpreted in the Markov model as: the observed variability in the boreholes at a certain scale (i.e., in the order of cm to m) in the boreholes must be present in the horizontal direction with a larger scale (i.e. in the order of 10 m to km).

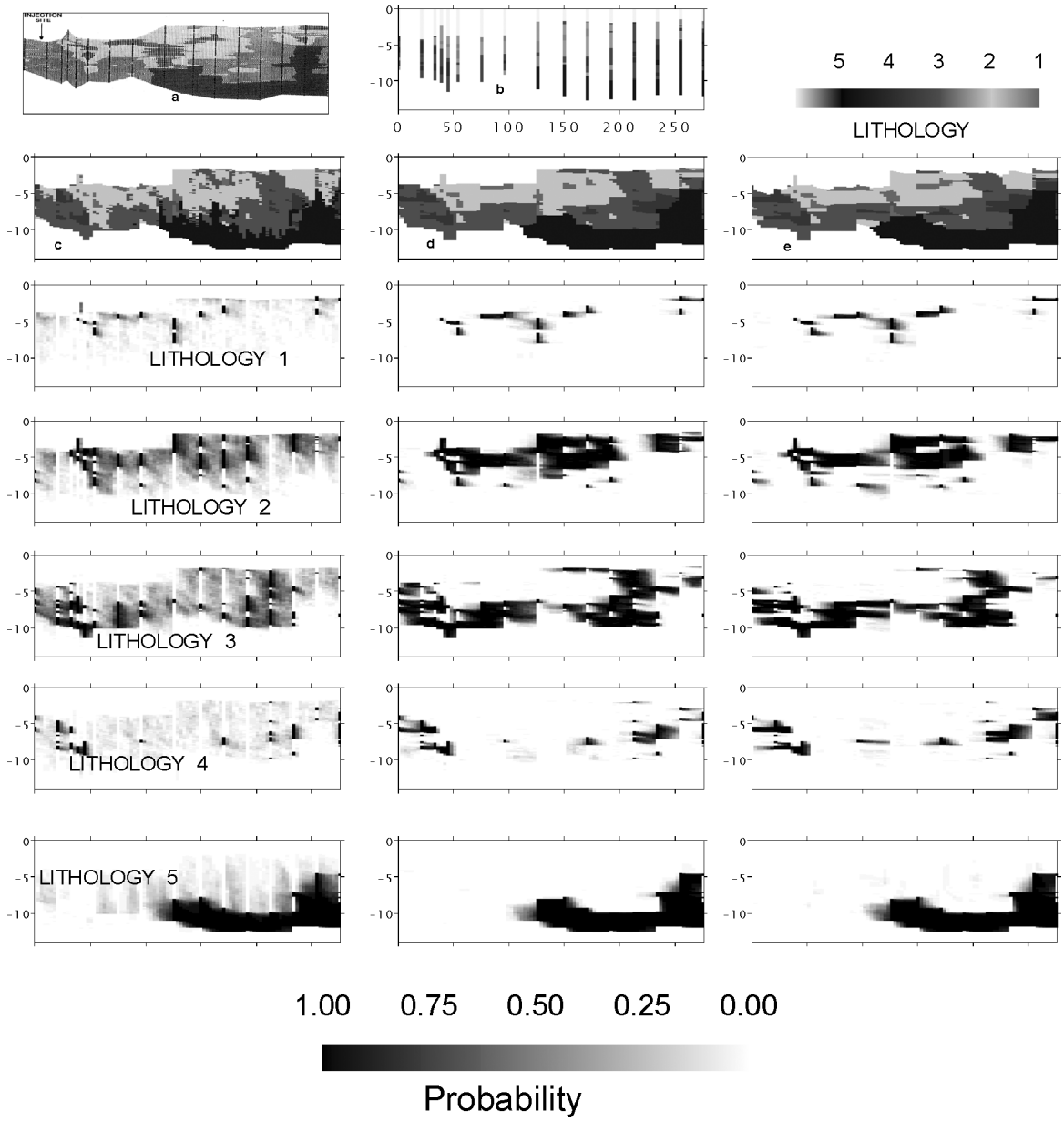


Figure 3(a) Comparison of different stochastic simulations of the MADE site, shown in (a), using the calculated vertical transition probability matrix, shown in Table 1, from the 16 boreholes (displayed in b), and assigning different horizontal transition probability matrices; (c) simulation by horizontal transition given in Table 2, (d) simulation by horizontal transition given in Table 3, (e) simulation by horizontal transition given in Table 4. The rest of images show the probability plots of each lithology under different transition probabilities.

## 5 Stochastic analysis of the geological realizations

The simulation results, in terms of final images, using the three matrices are presented in Fig. 3a(c,d,e) that correspond to the horizontal transitions given in Tables 2–4, respectively. The results show that the increase in the degree of diagonal dominancy of the horizontal transitions improves the simulation results in the sense that it gets closer to the image in Fig. 3(a-a). However, in the case of using the horizontal transition probabilities that are identical to the vertical transition probabilities, the results are satisfactory, except for state 1.

Maps of probability plots of each lithology are also presented in Fig. 3a(a) under different horizontal transition probability matrices. White color means perfect certainty that a lithology does not exist in this location, on the contrary black color means perfect certainty that a lithology exists in this location. Grey scale gives the probability of occurrence of a lithology at certain location. These plots show the increase of certainty by introducing more boreholes in the conditioning scenarios.

Figure 3(b) shows comparison of different stochastic simulations of the MADE site using the calculated vertical transition probability matrix from 16 boreholes (shown in Table 1) and assigning different horizontal transition probability matrices and different conditioning scenarios. Left column shows simulation by the horizontal transition probabilities given in Table 2 and conditioned on 6 boreholes, middle column shows simulation by the horizontal transition probabilities given in Table 3 and

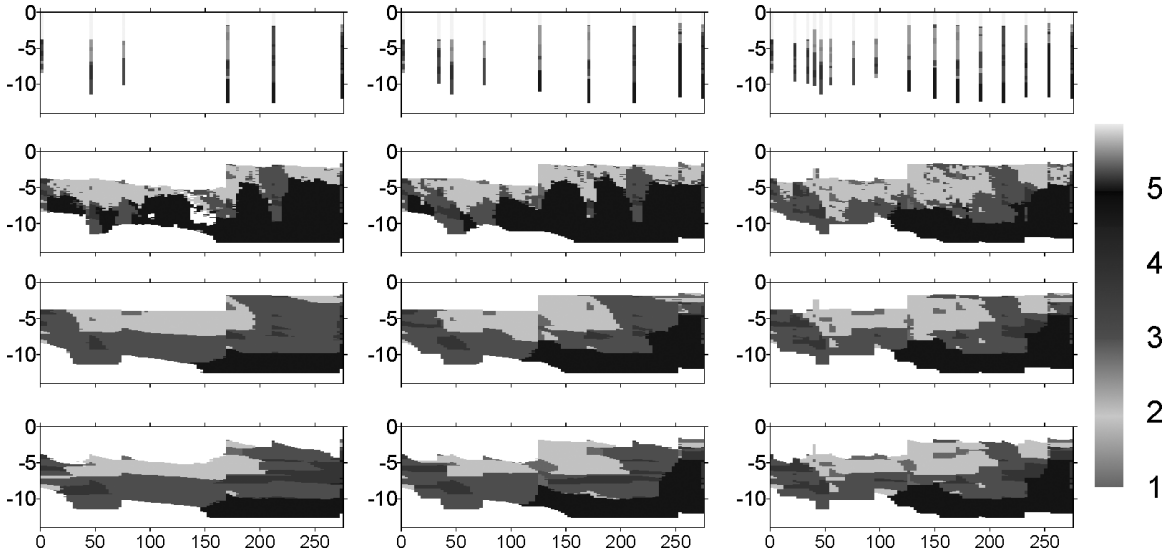


Figure 3(b) Comparison of different stochastic simulations of the MADE site using the calculated vertical transition probability matrix from 16 boreholes, shown in (Table 1) and assigning different horizontal transition probability matrices and different conditioning scenarios. Left column shows simulation by horizontal transition probabilities given in Table 2 and conditioned on 6 boreholes, middle column shows simulation by horizontal transition probability given in Table 3 and conditioned on 9 boreholes, right column shows simulation by horizontal transition probabilities given in Table 4 and conditioned on 16 boreholes.

Table 1 Vertical transition probability matrix sampled over 0.1 m Fig. 3a(b) (Elfeki and Rajabiani, 2002)

| State | State | | | | | | |
|---|---|---|---|---|---|---|---|
| | 1 | 2 | 3 | 4 | 5 | 6 | 7 |
| 1 | 0.879 | 0.103 | 0.009 | 0.000 | 0.009 | 0.000 | 0.000 |
| 2 | 0.026 | 0.911 | 0.046 | 0.009 | 0.003 | 0.000 | 0.005 |
| 3 | 0.003 | 0.030 | 0.897 | 0.044 | 0.010 | 0.000 | 0.016 |
| 4 | 0.000 | 0.006 | 0.094 | 0.869 | 0.031 | 0.000 | 0.000 |
| 5 | 0.000 | 0.000 | 0.003 | 0.010 | 0.961 | 0.000 | 0.026 |
| 6 | 0.009 | 0.014 | 0.009 | 0.005 | 0.000 | 0.963 | 0.000 |
| 7 | 0.000 | 0.000 | 0.000 | 0.000 | 0.000 | 0.000 | 1.00 |

Table 2 Forward horizontal transition probability Fig. 3a(c). Sampling in horizontal direction = 3 m (Elfeki and Rajabiani, 2002)

| State | State | | | | | | |
|---|---|---|---|---|---|---|---|
| | 1 | 2 | 3 | 4 | 5 | 6 | 7 |
| 1 | 0.500 | 0.100 | 0.100 | 0.100 | 0.100 | 0.100 | 0.000 |
| 2 | 0.100 | 0.500 | 0.100 | 0.100 | 0.100 | 0.000 | 0.100 |
| 3 | 0.100 | 0.100 | 0.500 | 0.100 | 0.100 | 0.000 | 0.100 |
| 4 | 0.100 | 0.100 | 0.100 | 0.500 | 0.100 | 0.000 | 0.100 |
| 5 | 0.100 | 0.100 | 0.100 | 0.100 | 0.500 | 0.100 | 0.000 |
| 6 | 0.001 | 0.001 | 0.001 | 0.001 | 0.001 | 0.994 | 0.001 |
| 7 | 0.001 | 0.001 | 0.001 | 0.001 | 0.001 | 0.001 | 0.994 |

Table 3 Forward horizontal transition probability Fig. 3a(d). Sampling in horizontal direction = 3 m (Elfeki and Rajabiani, 2002)

| State | State | | | | | | |
|---|---|---|---|---|---|---|---|
| | 1 | 2 | 3 | 4 | 5 | 6 | 7 |
| 1 | 0.879 | 0.103 | 0.009 | 0.000 | 0.009 | 0.000 | 0.000 |
| 2 | 0.026 | 0.911 | 0.046 | 0.009 | 0.003 | 0.000 | 0.005 |
| 3 | 0.003 | 0.030 | 0.897 | 0.044 | 0.010 | 0.000 | 0.016 |
| 4 | 0.000 | 0.006 | 0.094 | 0.869 | 0.031 | 0.000 | 0.000 |
| 5 | 0.000 | 0.000 | 0.003 | 0.010 | 0.961 | 0.000 | 0.026 |
| 6 | 0.009 | 0.014 | 0.009 | 0.005 | 0.000 | 0.963 | 0.000 |
| 7 | 0.000 | 0.000 | 0.000 | 0.000 | 0.000 | 0.000 | 1.00 |

Table 4 Forward horizontal transition probability (Fig. 3a(e)). Sampling in horizontal direction = 3 m (Elfeki and Rajabiani, 2002)

| State | State | | | | | | |
|---|---|---|---|---|---|---|---|
| | 1 | 2 | 3 | 4 | 5 | 6 | 7 |
| 1 | 0.922 | 0.015 | 0.015 | 0.015 | 0.015 | 0.015 | 0.003 |
| 2 | 0.015 | 0.922 | 0.015 | 0.015 | 0.015 | 0.015 | 0.003 |
| 3 | 0.015 | 0.015 | 0.922 | 0.015 | 0.015 | 0.015 | 0.003 |
| 4 | 0.015 | 0.015 | 0.015 | 0.922 | 0.015 | 0.015 | 0.003 |
| 5 | 0.015 | 0.015 | 0.015 | 0.015 | 0.922 | 0.015 | 0.003 |
| 6 | 0.015 | 0.015 | 0.015 | 0.015 | 0.015 | 0.922 | 0.003 |
| 7 | 0.001 | 0.001 | 0.001 | 0.001 | 0.001 | 0.001 | 0.994 |

conditioned on 9 boreholes, right column shows simulation by the horizontal transition probabilities given in Table 4 and conditioned on 16 boreholes. The simulation results show smoothing in the geological configuration (from top to bottom) with increasing the diagonal dominancy of the horizontal transition probability matrix. The simulation results capture more geological features when increasing the conditioning boreholes (from left to right).

Figure 4a shows three individual realizations and the final images produced using the final image approach at different conditioning scenarios. Although there is some variability over the realizations, the final images capture the main features of the MADE aquifer.

Figure 4b shows the variogram of $\ln(K)$ of the final images conditioned on the given boreholes in both $x$- and $y$-directions,

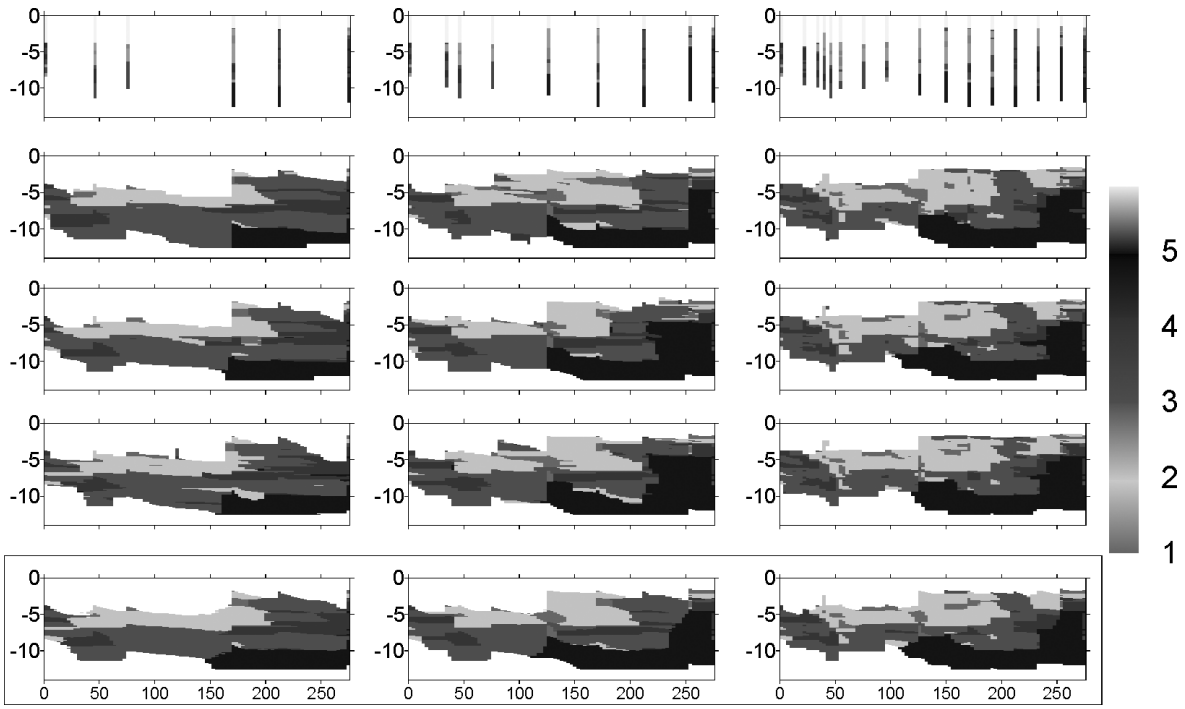


Figure 4(a) Comparison of individual realizations of the MADE site and the final images conditioned on 6, 9 and 16 boreholes. First row are boreholes, from second to forth row are three individual realizations conditioned on 6, 9 and 16 boreholes, respectively, from left to right. Last row are final images.

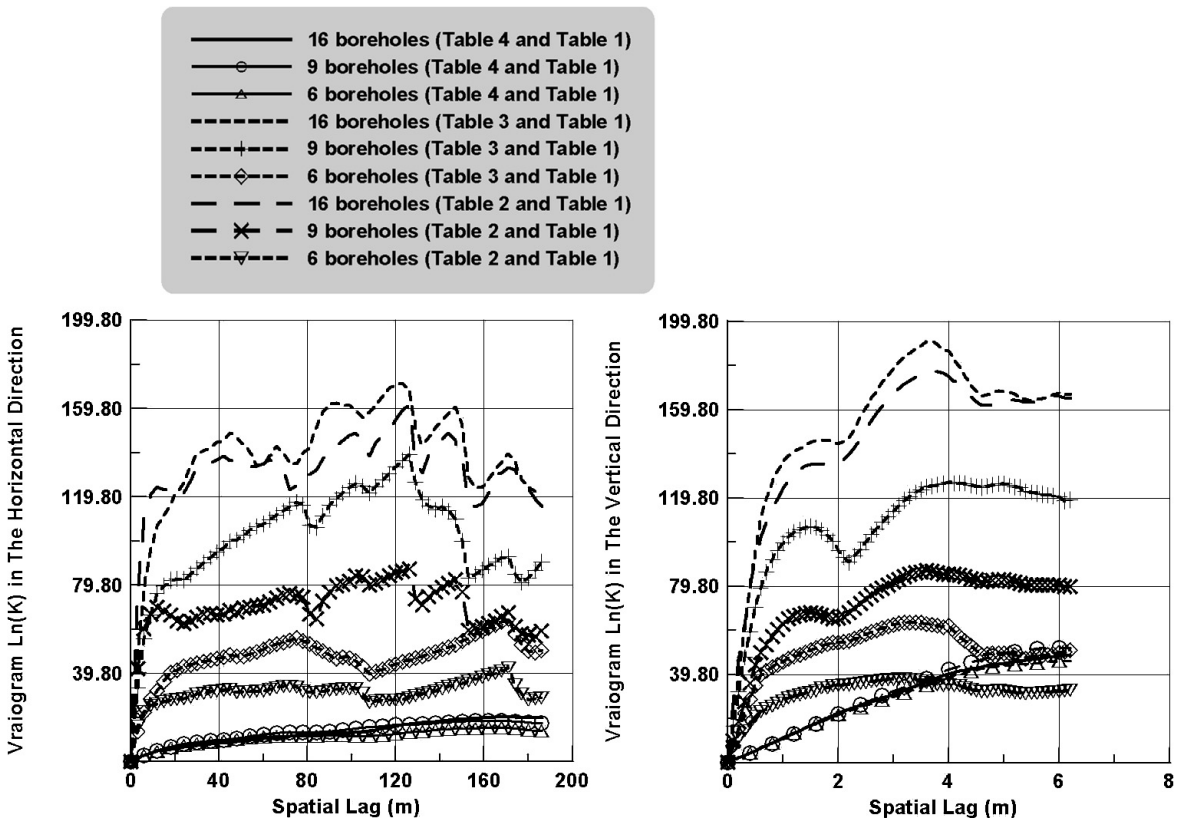


Figure 4(b) Comparison of ln($K$) variogram of the final images conditioned on 6, 9 and 16 boreholes in the horizontal (left ) and the vertical (right) directions, respectively, using different transition probability matrices.

respectively, using different transition probability matrices. The results show that variograms for transition probabilities given in Table 4 are almost identical under different conditioning scenarios and having the least variability.

The final image, that is produced from this approach, will be considered as a fixed image of the subsurface when flow and transport simulations are considered (Section 6). This is different from the traditional Monte Carlo approach used in Elfeki *et al.* (1998), where flow and transport are solved in each realization and outputs are averaged over the ensemble. The final image approach is, in some sense, similar to the simulations performed by Eggleston and Rojstaczer (1998) on a single realization.

## 6 Numerical simulations of the MADE1 experiment

Data used in the simulation of the field experiment are collected from available literature (e.g. Boggs *et al.*, 1990, 1992; Adams and Gelhar, 1992; Rehfeldt *et al.*, 1992). These data are summarized in Tables 5 and 6 together with the simulation parameters. Computer codes have been developed (Elfeki, 1996) to perform the simulations. It is worth mentioning that the hypothetical states 6 and 7 in the domain are assigned a very low conductivity value 0.0001 m/day. The code is a finite difference model that solves the steady state saturated groundwater flow equation in a heterogeneous medium under confined flow conditions with specified boundary conditions. The model considers the top and bottom of the domain as impermeable boundaries and the left and right sides as given head boundaries. The model calculates the hydraulic heads and the velocity field within the flow domain. A particle tracking random walk model has been developed to simulate solute transport in heterogeneous aquifers in saturated flow conditions. The random walk technique that is implemented in the code is based on the similarity of the transport equation and the Fokker–Planck equation (Uffink, 1990).

Some other assumptions have been made to perform flow and transport simulations at the MADE site: (1) The groundwater aquifer is assumed confined, which is not the case at the site. However, the top impermeable boundary is far from the hydraulic conductivity profile of the actual cross-section, this leads to some leakage from the top low conductive layer (represented in white in Figs 5 and 6) to the actual cross-section that may relieve this assumption. (2) Flow and transport is assumed to take place in a two-dimensional vertical domain, however it is three-dimensional in the site. The consequences of this assumption are explained by Burnett and Frind (1987). Therefore, some conclusions are made in a qualitative sense rather than in a quantitative sense. (3) The flow field is assumed steady. (4) Particles are placed initially at the location of the injection well and they are moved one by one in the medium according to the advective velocity and they disperse according to the pore-scale dispersion process. The effect of radial flow at the injection well is assumed negligible. This assumption can be justified by the fact that the radial flow, which is created around the well for the period of the injection (about 48 h), which is very small, compared to the time scale of the experiment (>500 days).

Table 5 Hydraulic conductivity values assigned to facies (lithofacies definitions from Rehfeldt *et al.*, 1992 and lithofacies values from Adams and Gelhar, 1992, Fig. 2)

| Facies | Measured Conductivity (m/day) | | |
|---|---|---|---|
| | Lower limit | Upper limit | Mid-range |
| 1. Open work gravel | 86.4 | 864.0 | 475.2 |
| 2. Fine gravel | 8.64 | 86.4 | 47.52 |
| 3. Sand | 0.864 | 8.64 | 4.752 |
| 4. Sandy gravel | 0.0864 | 0.864 | 0.4752 |
| 5. Sandy clayey gravel | 0.00864 | 0.0864 | 0.04752 |

Table 6 Numerical values used in the simulation of the tracer experiment (modified from Elfeki and Rajabiani, 2002)

| Parameter | Numerical value |
|---|---|
| Domain dimensions | Lx = 276 m, Ly = 14.2 m |
| Domain discretezation | DX = 3 m, DY = 0.1 m |
| Average head difference at the site | 0.7 m |
| Mean flow direction | Left to right, under gradient = 0.0025 |
| Injected tracer mass of bromide | 2.5 kg |
| Number of particles | 1,000,000 particles |
| Time step in calculations | 0.5 day |
| Longitudinal pore-scale dispersivity | 0.10 m (no data available) |
| Transverse pore-scale dispersivity | 0.01 m (no data available) |
| Effective porosity | 0.35 (Adams and Gelhar, 1992; Table 1) |
| Average aquifer thickness | 10 m |
| $X$-coordinate of injection | 12 m |
| Initial solute body dimensions (rectangular in shape) | Width = 0.2 m and depth = 4.0 m |
| Molecular diffusion coefficient | 0.0 (no data available) |
| Retardation coefficient | 1.0 |

Table 7(a) shows the proportion of each lithology in the MADE simulation under the three conditioning scenarios. The table shows that the proportion of lithology no. 1 and 2 (high conductivity) increases with increasing the number of conditioning boreholes. Similarly, lithology no. 5 (low conductivity) increases with increasing the number of conditioning boreholes. Lithology no. 3 and 4 (medium to low conductivity) decrease with increasing the number of conditioning boreholes. The table shows some convergence of the proportions to certain values. These proportions have consequences on calculations of averages as seen in the next table.

Table 7(b) summarizes the spatial weighted average conductivities, variances of the three conditioning scenarios with upper, lower and mid-range conductivities shown in Table 5 and the estimated values from the MADE site (Rehfeldt *et al.*, 1992, Tables 2 and 3). The average log-conductivity values obtained from the three scenarios are almost the same. The averages are almost

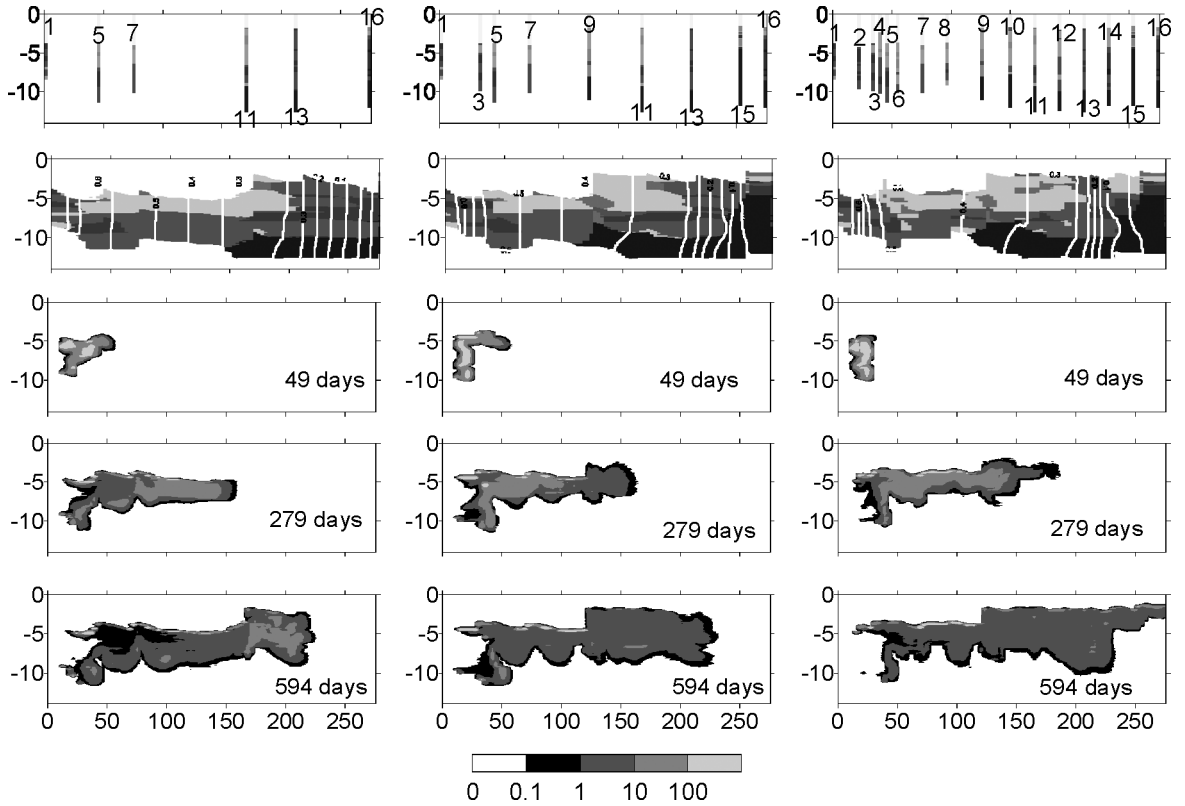


Figure 5(a) Comparison of numerical flow and transport simulations conditioned on the number of boreholes with upper conductivity limits. Left most column is a geological simulation of the aquifer conditioned on 6 boreholes with the corresponding flow field and plume evolution at 49, 279 and 594 days, respectively. Second and third columns are similar to left most column but conditioned on 9 and 16 boreholes, respectively. The concentration scale is in mg/L.

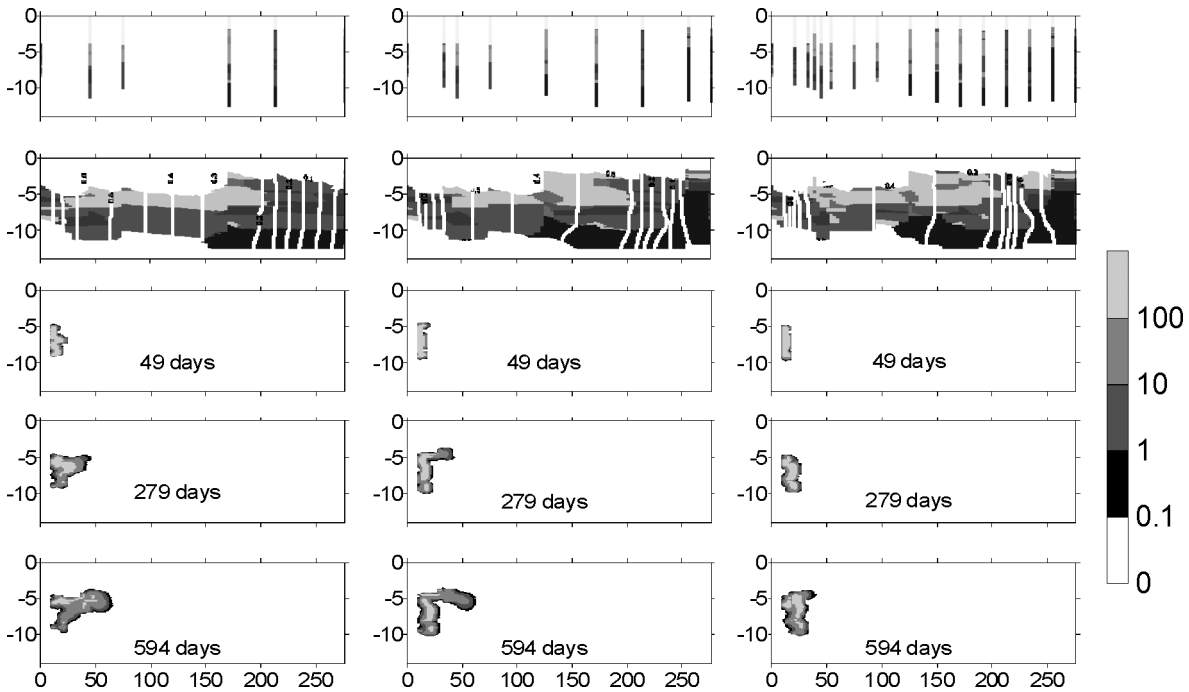


Figure 5(b) Comparison of numerical flow and transport simulations conditioned on the number of boreholes with lower conductivity limits. Left most column is a geological simulation of the aquifer conditioned on 6 boreholes with the corresponding flow field and plume evolution at 49, 279 and 594 days, respectively. Second and third columns are similar to left most column but conditioned on 9 and 16 boreholes, respectively. The concentration scale is in mg/L.

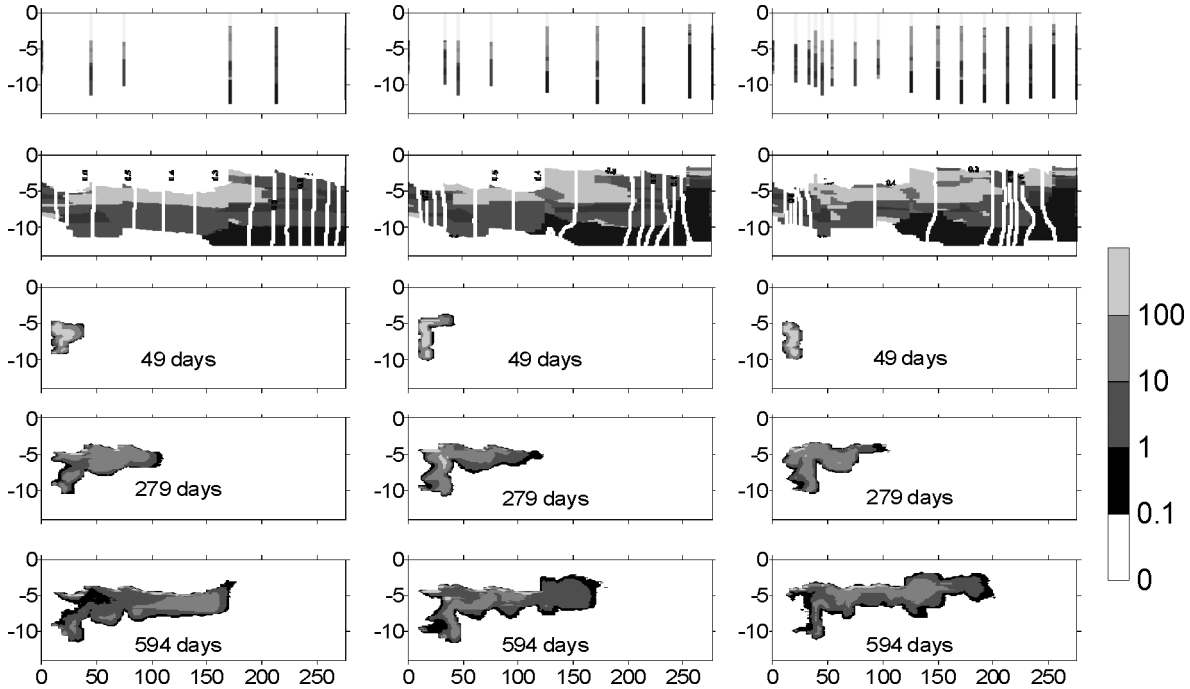


Figure 5(c) Comparison of numerical flow and transport simulations conditioned on the number of boreholes with mid range conductivity. Left most column is a geological simulation of the aquifer conditioned on 6 boreholes with the corresponding flow field and plume evolution at 49, 279 and 594 days, respectively. Second and third columns are similar to left most column but conditioned on 9 and 16 boreholes, respectively. The concentration scale is in mg/L.

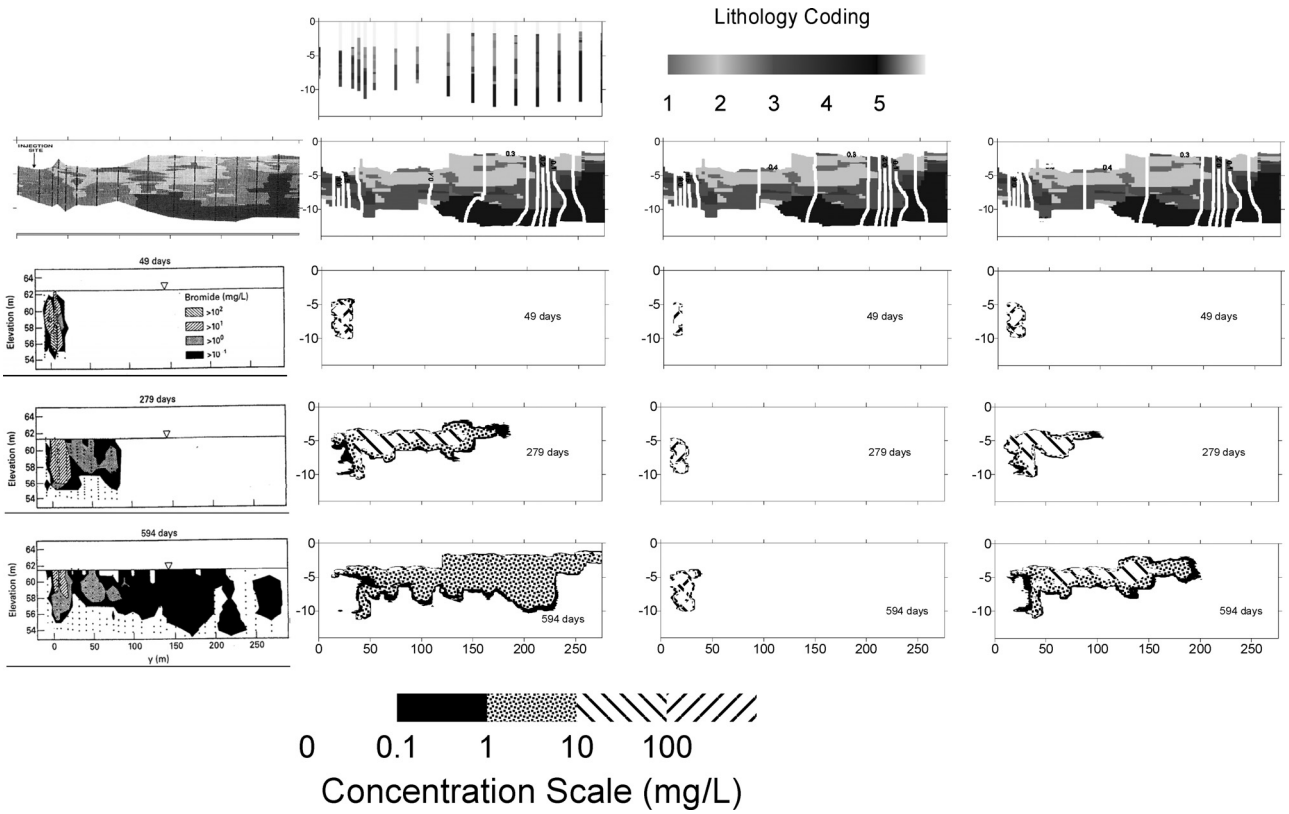


Figure 6 Numerical flow and transport simulations of the MADE1 experiment. Left column shows the data (Boggs *et al.*, 1990, 1992). The two middle and right columns show simulation results under upper, lower and mid-range conductivities, respectively.

Table 7a Comparison of the proportion of each lithology in the cross-section when conditioned on number of boreholes

| Lithology | 16 Boreholes | 9 Boreholes | 6 Boreholes |
|---|---|---|---|
| 1 | 0.046 | 0.038 | 0.012 |
| 2 | 0.258 | 0.207 | 0.205 |
| 3 | 0.327 | 0.380 | 0.479 |
| 4 | 0.097 | 0.109 | 0.141 |
| 5 | 0.273 | 0.267 | 0.163 |

Table 7b Comparison of statistics computed from the three scenarios (this study, with upper, lower and mid-range conductivities) and the values estimated from the MADE site (Rehfeldt *et al.*, 1992, Tables 2 and 3)

| Parameter | 16 Boreholes | 9 Boreholes | 6 Boreholes | MADE data |
|---|---|---|---|---|
| $\mu_{\ln(K)}$ | −5.28 (upper) | −5.44 (upper) | −5.15 (upper) | −5.2 |
| | −5.87 (mid-range) | −6.03 (mid-range) | −5.75 (mid-range) | (−10.1–0.4) |
| | −7.68 (lower) | −7.43 (lower) | −7.47 (lower) | |
| $\sigma^2_{\ln(K)}$ | 8.19 (upper) | 7.43 (upper) | 5.25 (upper) | 4.5 |
| | 8.19 (mid-range) | 7.43 (mid-range) | 5.25 (mid-range) | (3.4–5.6) |
| | 7.31 (lower) | 7.43 (lower) | 5.03 (lower) | |

the same as the values obtained from Rehfeldt *et al.*, (1992) under the upper conductivity limits. The mid-range and lower conductivities are within the estimation limits. The variances of log-conductivities are more than the one estimated by Rehfeldt *et al.* (1992), and are also outside the estimated limits. This is probably due to the choice of one single value to represent the entire lithology from Adams and Gelhar (1992), however, the estimated values from Rehfeldt *et al.* (1992) are based on 2187 measurements.

## 7 Flow and Transport Simulation results

Figure 5(a–c) shows the comparison of the simulated hydraulic head field and the plume shapes at specified snapshots (49, 279 and 594 days), conditioned on 6, 9 and 16 boreholes, respectively, under upper, lower and mid-range hydraulic conductivities as given in Table 5. Figure 5(a) shows simulations under upper conductivity limits. The results capture the hydraulic head field reasonably well, even with a reduced number of conditioning boreholes. Conditioning on 9 boreholes satisfactorily represents plume shapes. In the case of 6 boreholes the results are different at the near field, however, the results improved at the far field to some extent. Figure 5(b) shows simulation results under lower conductivity limits. The head contours do not change that much from the upper conductivity case because the ratio between the upper and lower limits is the same for each lithology. The plume is very slow. It does not move far way from the injection location. Figure 5(c) shows simulations under mid-range conductivity. The plumes look very similar in shapes under various conditioning scenarios. The effect of conductivities appears in the figures. At low conductivity the plume is very slow, at high conductivity the plume is fast, and at the mid-range conductivity the plume is relatively fast.

Figure 6 shows the hydraulic head distribution, plume data and simulation results with upper, lower and mid-range hydraulic conductivities in terms of plume concentrations at specified times 49, 279 and 594 days, respectively, conditioned on 16 boreholes. The simulation results reproduced many features of the flow field and the plume behavior, e.g. closely spaced hydraulic head contours in the near-field are observed, however in the far-field there is widely spaced hydraulic head contours. Skewed concentration distribution in the longitudinal direction and large vertical spreading of the plume at the vicinity of the injection well are also observed. The simulation starts with an initial vertical dimension of the plume of 4 m. This vertical dimension increases significantly in time, although lateral dispersivity is very small (0.01 m). This is due to natural upward vertical gradients present in the vicinity of the injection site. Maximum bromide concentrations of the bromide profile at 594 days were located in the upper part of the plume as were observed at the site. Reduction of the plume thickness that occurring between approximately 20 and 40 m down gradient from the injection point is also noticed. The final image of the lithological units with mid-range and upper hydraulic conductivities seem to capture both the flow field and the plume shape of the real field.

Figure 7(a) shows the evolution of the centroid of the plume conditioned on 6, 9 and 16 boreholes under the upper, lower and mid-range conductivities, the field-estimated values and the simulation results conducted by Eggleston and Rojstaczer (1998). The first moment shows overestimation of plume evolution with respect to the field computed values under the upper and mid-range conductivities together with the polynomial trend used by Eggleston and Rojstaczer (1998). However, it shows underestimation of the simulation results under the lower conductivity limits together with Kriging, filtered trend, and sediment zone used by Eggleston and Rojstaczer (1998). The reason is the wide range of values of the conductivity of each geological unit [i.e. the high uncertainty in the hydraulic conductivity values (Table 5)] and/or the uncertainty of the value of the effective porosity. In general, the field-estimated values lie in between the bounds of the conductivity values given in Table 5. The results reflect the uncertainty in the conductivity values on the plume first spatial moment.

Figure 7(b) presents the evolution of the longitudinal variance ($x$-direction) of the plume conditioned on 6, 9 and 16 boreholes, respectively, under upper, lower and mid-range conductivities, the field-estimated values and the simulation results conducted by Eggleston and Rojstaczer (1998). The second moment shows a superdiffusive regime [i.e. the growth of the longitudinal variance is faster than linear in time (Sahimi, 1993)] under upper

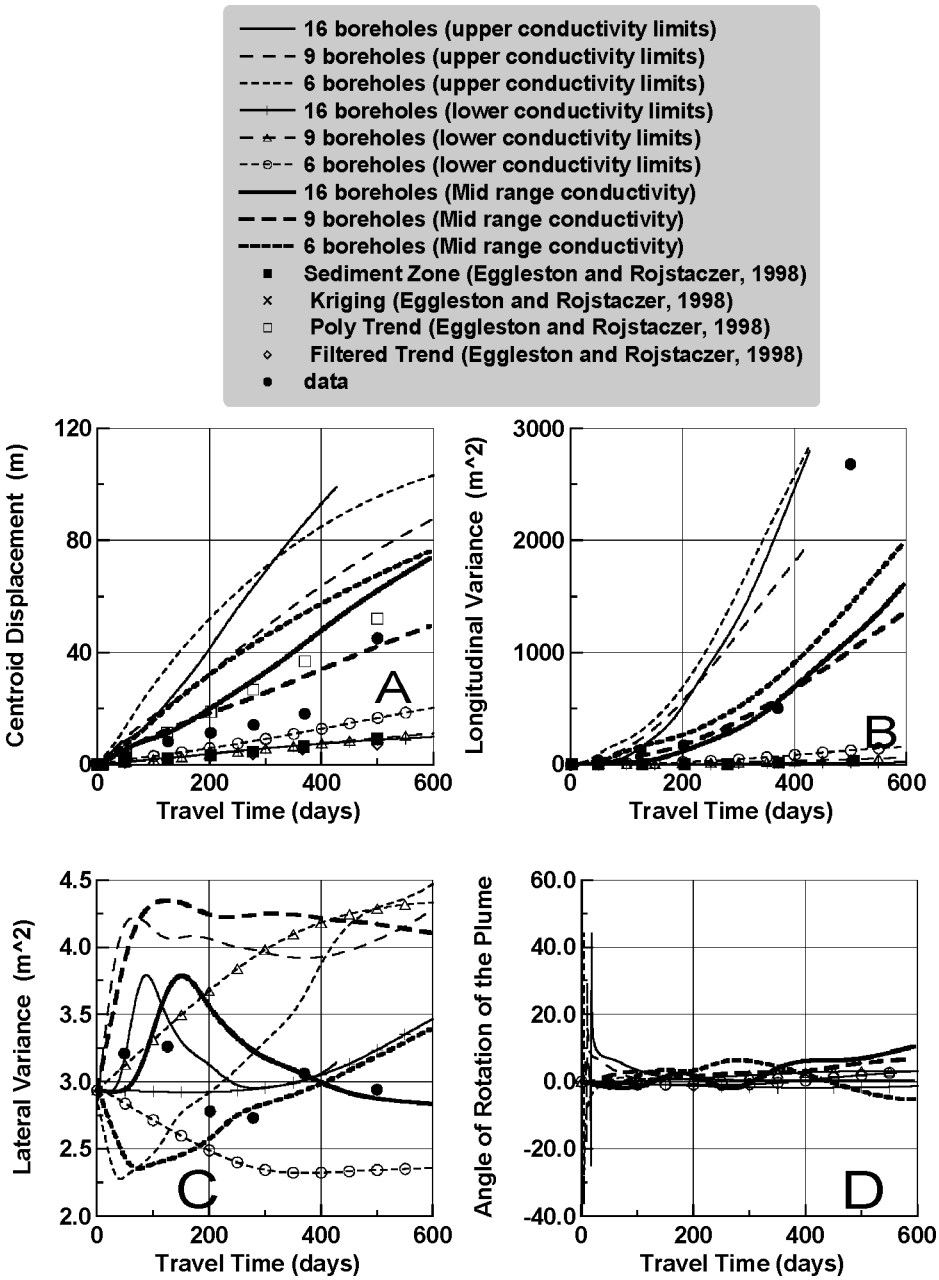


Figure 7 Comparison of plume spatial moments conditioned on the number of boreholes: (a) is the evolution of the $x$-coordinate of the plume centroid, (b) is the evolution of the longitudinal variance, (c) is the evolution of the lateral variance, (d) is the evolution of the angle of rotation of the plume.

and mid-range conductivities when compared with the field-computed values. This behavior is justified by the conductivity contrast and the layering effect that lead to preferential flow paths in the far field. However, there are a few discrepancies due to the geometrical configuration created by conditioning on 6, 9 and 16 boreholes. The mid-range conductivity seems to capture the field-computed second moments fairly well. The lower conductivity limits show very slow growth in the longitudinal variance that is close to the values predicted by Eggleston and Rojstaczer (1998). However, in general the field-estimated values lie within the bounds of the conductivity values.

Figure 7(c) displays the evolution of the lateral variance ($y$-direction) of the plume conditioned on 6, 9 and 16 boreholes, respectively, under the upper, lower and mid-range conductivities and the field-estimated values. The graph shows significant variations due to convergent and divergent flow lines. The plume shrinks laterally where there is convergence in the flow lines while it expands laterally where there is divergence in the flow lines. This behavior is reflected in the figure. Data on Fig. 7(c) are also plotted in the graph after calibrating on the initial plume size. It shows that conditioning on 16 boreholes is providing best results in the lateral spreading of the plume under upper and mid-range conductivities.

Figure 7(d) shows the evolution of the angle of rotation of the plume in degrees conditioned on 6, 9 and 16 boreholes, respectively, under the upper, lower and mid range conductivities. At early stages, the plume shows different orientations. However, in the far field, after about 100 days the plume moves almost horizontally in the three cases. There were no data available on Fig. 7(d). The only available data is the angle of rotation in the

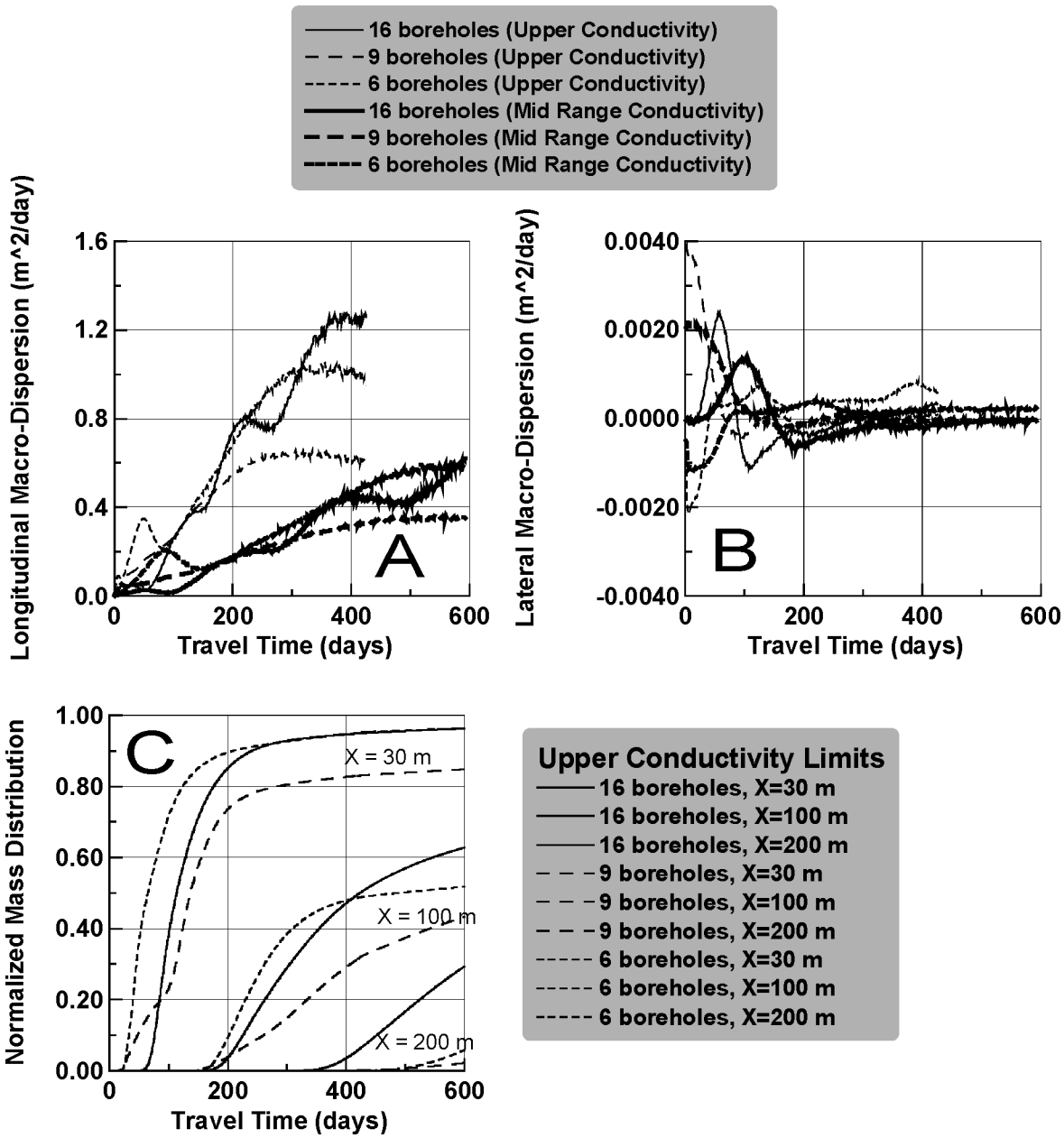


Figure 8 Comparison of plume dispersion and breakthrough curves conditioned on the number of boreholes. Dispersion is plotted with upper and mid-range conductivity limits, while breakthrough curves are plotted with upper conductivity limits: (a) shows the evolution of longitudinal dispersion, (b) shows the evolution of lateral dispersion, (c) shows the breakthrough curves at 30, 100 and 200 m from the source.

horizontal plane (Adams and Gelhar, 1992), while the simulation presented here is the angle of rotation in the vertical plane. However, visual observation of the plume confirms horizontal movement in the far field in the vertical plane (see Fig. 6 left most column).

Figure 8(a) displays the evolution of the macrodispersion coefficient of the plume in the $x$-direction conditioned on 6, 9 and 16 boreholes, respectively, under upper and mid-range conductivities. The macrodispersion of the lower conductivity is not computed because the plume is not fully developed. The macrodispersion coefficient is calculated by taking half the derivative of the longitudinal variance in time. This way of calculation is similar to the approach followed by Adams and Gelhar (1992) (Eq. 10 in their paper). The results show non-monotonic increase of the macrodispersion coefficient. This is due to the highly non-uniform flow pattern at the site, which is characterized by convergent and divergent flows in the near and far fields. This behavior has been supported by previous work (Elfeki *et al.*, 1996). This makes it difficult to define an asymptotic marcodispersion. However, we tried to get some estimates by taking an asymptote at the maximum value in the curve, and comparing the results with Gelhar's theory (Adams and Gelhar, 1992), that accounts for some features of non-uniform flow (see Table 8). The results of the longitudinal macrodispersivities are in an order of magnitude of the observed ones. However, Gelhar's theory underestimates the observed values. There are discrepancies between the values of macrodispersivites obtained by conditioning on 6, 9 and 16 boreholes. The reason is that each macrodispersivity corresponds to a certain geological configuration which is obtained based on

Table 8 Observed, predicted and simulated Macrodispersivities (with upper and mid-range conductivities)

| Dispersivity (m) | Observed | Adams and Gelhars (1992) | This study | | |
|---|---|---|---|---|---|
| | | | 16 Boreholes | 9 Boreholes | 6 Boreholes |
| $A_{11}$ | 5–10 | 1.48–1.5 | 13.25 (upper)<br>4.3 (mid-range) | 8.75 (upper)<br>4.7 (mid-range) | 16.18 (upper)<br>4.5 (mid-range) |
| $A_{33}$ | Not computed | <0.005 | 0.005 (upper)<br>~0 (mid-range) | 0.003 (upper)<br>~0 (mid-range) | 0.0016 (upper)<br>0.0015 (mid-range) |

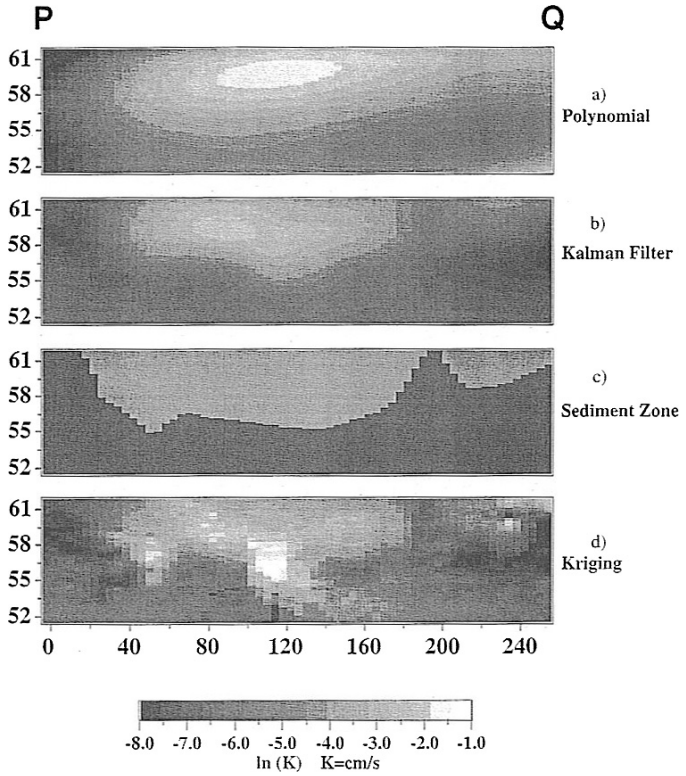


Figure 9 Hydraulic conductivity maps, vertical cross-section, generated by: (a) polynomial regression, (b) Kalman filtering, (c) sedimentation zone and (d) Kriging (from Eggleston and Rojstaczer, 1998; Fig. 6).

conditioning on 6, 9 and 16 boreholes. Therefore, increasing the number of conditioning boreholes from 6 to 16 does not lead to converge to the same macrodispersion coefficient (see Table 8). Figure 8(b) presents the evolution of the macrodispersion coefficient of the plume in the *y*-direction under upper and mid-range conductivity values. The results show very small values that are practically zero. This finding is supported by a Monte Carlo analysis performed by Elfeki *et al.*, (1998). The lateral macrodispersivity values are in the same order of magnitude as the ones obtained by Gelhar's theory (Table 8).

Figure 8(c) presents breakthrough curves at some locations in the aquifers (30, 100 and 200 m from the source), conditioned on 6, 9 and 16 boreholes under upper conductivity values. These curves show average behavior over the depth of the aquifer. The breakthrough conditioned on 16 boreholes lies in the middle of the two cases conditioned on 9 boreholes (slowest case) and conditioned on 6 boreholes (fastest case). The curves show pronounced non-Gaussian behavior of the breakthrough with steep fronts and long tails which is common for highly heterogonous deposits.

Figure 9 shows results of the work reported in the literature by Eggleston and Rojstaczer (1998) regarding characterization of the MADE site using various methods such as polynomial regression trend, Kalman filter trend, sediment zone and Kriging. Comparison of the CMC simulation results (Fig. 3a–e) and simulation results by Eggleston and Rojstaczer (1998) presented in Fig. 9 prove that CMC is a lot better in characterizing the MADE site.

## 8 Conclusions

Some conclusions can be drawn from this study:

1. The CMC model has shown successful results in delineating the complex geological configuration of the aquifer at the MADE site (Fig. 3a-a) when the system was conditioned on the observed 16 boreholes (Fig. 3a-e).
2. The forward horizontal transition probability matrix given in Table 4 is capable of capturing the main features of the Columbus site when conditioned on the given 16 boreholes. Values of the diagonal elements of the horizontal transition probability matrix which have been taken equal to 0.922 for the facies are sufficient to produce the main heterogeneous features at the site (Elfeki and Rajabiani, 2002).
3. Flow and transport simulations capture the salient features of the flow field and the large-scale plume behavior at the site. This means that delineation of the large-scale geological configuration coupled with the correct values of the hydraulic parameters is crucial to obtain satisfactory simulation results. In MADE1 experiment, the mid-range conductivity provides satisfactory results with respect to plume shape and spatial second moments. The fist spatial moment is still overestimated which may be due to underestimation of the porosity value.
4. The transport mechanisms predicted by the model, under upper conductivity limits, for the three different conditioning scenarios show a superdiffusive regime. This is due to the preferential flow paths and the dimensionality of the problem. The 2D model overestimates the macrodispersivities when compared with the ones obtained by Gelhar's theory.

5. The final images that were obtained based on conditional realizations on 16, 9 and 6 boreholes show reasonably the same plume behavior in terms of average longitudinal and vertical extensions (Fig. 5a,c) under the upper and mid-range conductivity values; 9 boreholes seem to provide practically acceptable results in terms of the global plume shape. This indicates more reliability on the use of the CMC model for subsurface characterization.
6. All plume spatial moments of the MADE site fall within the bound of the simulated spatial moments under the upper and lower limits of the conductivity values. The bound reflects high uncertainty of the hydraulic conductivity of each lithology.
7. Comparison of CMC model results (Fig. 3(a)a-e) with the results of Eggleston and Rojstaczer (1998) presented in Fig. 9 using different models (polynomial regression trend, Kalman filter trend, hydrofacies trend and Kriging) shows that CMC model performs better in terms of delineating the geological configuration of the MADE site.

## Acknowledgments

This research work is supported by the DIOC Water project of Delft University of Technology, Delft, The Netherlands. The author would like to thank Prof. Dekking from Faculty of EEMCS, Delft University of Technology, Delft, The Netherlands for commenting on the manuscript. I would like also to acknowledge Mr. Rajabiani for the preliminary runs he performed by the model code in his MSc Thesis. The author would like to thank the anonymous reviewers for their valuable comments.

## References

1. ADAMS, E.E. and GELHAR, L.W. (1992). "Field Study of Dispersion in a Heterogeneous Aquifer, 2 Spatial Moment Analysis". *Water Resour. Res.* 28(12), 3293–3307.
2. BOGGS, J.M., YOUNG, S.C., BENTON, D.J. and CHUNG, Y.C. (1990). *Hydrogeological Characterization of the MADE Site*. Top. Rep. EN-6915, Electric Power Research Institute, Palo Alto, CA.
3. BOGGS, J.M., YOUNG, S.C., BEARD, L.M., GELHAR, L.W., REHFELDT, K.R. and ADAMS, E.E. (1992). "Field Study of Dispersion in a Heterogeneous Aquifer, 1 Overview and Site Description". *Water Resour. Res.* 28(12), 3281–3291.
4. BURNETT, R.D. and FRIND, E.O. (1987). "Simulation of Contaminant Transport in Three Dimensions: 2. Dimentionality Effects". *Water Resour. Res.* 23(4), 695–705.
5. CROSS, G.R. and JAIN, A.K. (1983). "Markov Random Field Texture Models". *IEEE Trans. Pattern Analysis Machine Intelligence* 5(1), 105–117.
6. EGGLESTON, J. and ROJSTACZER, S. (1998). "Identification of Large-scale Hydraulic Conductivity Trends and the Influence of Trends on Contaminant Transport". *Water Resour. Res.* 34(9), 2155–2168.
7. ELFEKI, A.M.M. (1996). "Stochastic Characterization of Geological Heterogeneity and Its Impact on Groundwater Contaminant Transport". PhD Thesis, Delft University of Technology, Delft, The Netherlands, 301 pp.
8. ELFEKI, A.M.M. and DEKKING, F.M. (2001). "A Markov Chain Model for Subsurface Characterization: Theory and Applications". *Math. Geol.* 33(5), 569–589.
9. ELFEKI, A.M.M. and DEKKING, F.M. (2005). "Modeling Subsurface Heterogeneity by Coupled Markov Chains: Directional Dependency, Walther's law and Entropy". *Journal of Geotechnical and Geological Engineering* 23, 721–756.
10. ELFEKI, A.M.M. and RAJABIANI, H.R. (2002). "Simulation of Plume Behavior at the Macrodispersion Experiment (MADE1) Site by Applying the Coupled Markov Chain Model for Site Characterization". *14th International Conference Computational Methods in Water Resources "CMWR2002"*, Delft, The Netherlands. Elsevier Publisher, Amsterdam, pp. 655–662.
11. ELFEKI, A.M.M., UFFINK, G.J.M. and BARENDS, F.B.J (1996). "Solute Transport in Single and Multiple Scale Heterogeneous Formations: Numerical Experiments". In: SOARES, A., HERNANDEZ, J. and FROIDEVAUX, R. (eds), *Geoenv 96, First European Conference on Geostatistics for Environmental Applications, Lisbon, Portugal*. Kluwer Academic Publishers, Dordrecht, pp. 51–63.
12. ELFEKI, A.M.M., UFFINK, G.J.M. and BARENDS, F.B.J. (1997). *Groundwater Contaminant Transport: Impact of Heterogeneous Characterization: A New View on Dispersion*. Balkema Publisher, The Netherlands, 301 pp.
13. ELFEKI, A.M.M., UFFINK, G.J.M. and BARENDS, F.B.J. (1998). "A Coupled Markov Chain Model for Quantification of Uncertainty in Transport in Heterogeneous Formations". In: SOARES, A. and HERNANDEZ, J. (eds), *GeoENV 98, Second European Conference on Geostatistics for Environmental Applications*. Kluwer Academic Publishers, Dordrecht, pp. 256–270.
14. GALBRAITH, R.F. and WALLEY, D. (1976). "On a Two-dimentional Binary Process". *J. Appl. Probab.* 13, 548–557.
15. HESS, K.M., WOLF, S.H. and CELIA, M.A. (1992). "Large-scale Natural Gradient Tracer Test in Sand and Gravel, Cape Cod, Massachusetts, 3 Hydraulic Conductivity and Calculated Macrodispersivities". *Water Resour. Res.* 28, 2011–2027.
16. KESHTA, N.A.R. (2003). "An Application of Stochastic Models in Groundwater Pollution Transport". MSc Thesis, Faculty of Engineering, Mansoura University, Mansoura, Egypt, 145 pp.
17. KESHTA, N.A.R., ZIDAN, A.-R.A., EZZELDIN, M.M. and ELFEKI, A.M. (2004). "Stochastic Analysis of Subsurface Heterogeneity Using Markov Chains: A Case Study in The Netherlands". In: EL-NMIR *et al.* (eds), *Structural & Geotechnical Engineering and Construction Technology Conference*, IC-SGECT'04. Mansoura University Press, Mansoura, Egypt, pp. c-415–c-423.

18. LI, W., ZHANG, C., BURT, J.E., ZHU, A.-X. and FEYEN, J. (2004). "Two-dimensional Markov Chain Simulation of Soil Type Spatial Distribution". *Soil Sci. Soc. Am. J.* 68, 1479–1490.
19. MIDDLETON, G.V. (1973). "Johannes Walther's Law of the Correlation of Facies". *Geol. Soc. Am. Bull.* 84, 979–988.
20. RAJABIANI, H.R. (2001). "Characterization of Subsurface Heterogeneity from Boreholes with Coupled Markov Chain for Groundwater Transport". MSc Thesis, Faculty of Civil Engineering and Geosciences, Delft University of Technology, Delft, The Netherlands, 76 pp.
21. REHFELDT, K.R., BOGGS, J.M. and GELHAR, L.W. (1992). "Field Study of Dispersion in a Heterogeneous Aquifer, 3 Geostatistical Analysis of Hydraulic Conductivity". *Water Resour. Res.* 28(12), 3309–3324.
22. PARKS, K.P., BENTLEY, L.R. and CROWE, A.S. (2000). "Capturing Geological Realism in Stochastic Simulations of Rock Systems with Markov Statistics and Simulated Annealing". *J. Sedi. Res.* 70(4), 803–813.
23. PARK, E., ELFEKI, A.M.M. and DEKKING, F.M. (2005). Characterization of subsurface heterogeneity: Integration of soft and hard information using multi-dimensional Coupled Markov chain approach. Chapter 16 in *Underground Injection Science and Technology Symposium*, eds. TSANG, C.-F. and APPS, J.A., Developments in Water Sciences Series 52, ISBN 13:978-0-444-52068-5, pp. 193–202.
24. SAHIMI, M. (1993). "Fractal Superdiffusion Transport and Hydrodynamic Dispersion in Heterogeneous Porous Media". *Transport Porous Media* 13, 3–40.
25. SUDICKY, E.A. (1986). "A Natural Gradient Experiment on Solute Transport in a Sand Aquifer: Spatial Variability of Hydraulic Conductivity and Its Role in the Dispersion Process". *Water Resour. Res.* 22(13), 2069–2082.
26. UFFINK, G.J.M. (1990). "Analysis of Dispersion by the Random Walk Method". PhD Thesis, Delft University of Technology, Delft, The Netherlands, 200 pp.
27. ZHENG, C. and JIAO, J.J. (1998). "Numerical Simulation of Tracer Tests in a Heterogeneous Aquifer". *J. Environ. Engng.* 124(6), 510–516.